Fast nonthermal processes in pulsed laser deposition

Jeffrey G. Ulbrandt, Xiaozhi Zhang ©, and Randall L. Headrick ©[*]
Department of Physics and Materials Science Program, University of Vermont, Burlington, Vermont 05405, USA

Rui Liu © and Matthew Dawber
Department of Physics and Astronomy, Stony Brook University, Stony Brook, New York 11794, USA

Kenneth Evans-Lutterodt
National Synchrotron Light Source II, Brookhaven National Laboratory, Upton, New York 11967, USA

Pulsed laser deposition (PLD) is widely used to grow epitaxial thin films of quantum materials. Here, we use *in situ* x-ray scattering to study homoepitaxy of $SrTiO_3$ by energetic deposition (e-PLD) versus PLD thermalized by a He background gas (th-PLD). Energetic PLD suppresses the lateral growth of two-dimensional islands, which suggests that particles with kinetic energies of $\sim$100 eV break up smaller islands. Fast interlayer transport occurs for th-PLD as well as e-PLD, implying a process operating on submicrosecond time scales for incident particles with kinetic energies below 10 eV.

Pulsed laser deposition (PLD) is a versatile method for homoepitaxial growth of ultrasmooth crystalline surfaces [1], heteroepitaxial interfaces [2–4], and superlattices [5]. Understanding and controlling the growth processes occurring in PLD and other energetic deposition methods presents an important challenge for the synthesis of thin layers with controllable properties.

PLD employs microsecond-scale pulses that occur as the laser plume reaches the growth surface, resulting in instantaneous deposition rates orders of magnitude higher than in continuous deposition methods such as molecular beam epitaxy (MBE). Deposited particles cannot diffuse a significant lateral distance on the surface while the rest of the plume is arriving. This is generally true over a wide range of deposition temperatures in the layer-by-layer growth regime, which is most relevant to epitaxial growth. Thus it becomes possible to study fast microscopic crystallization mechanisms separately from slower thermal relaxation effects by studying the evolving x-ray scattering intensity on the relevant timescales.

Here, we show the effects of varying the energy distribution of the particles in the laser plume produced by a 248 nm excimer laser. At low background gas pressures, the ablated particles reach the growth surface with high kinetic energies, a process which we call e-PLD. The kinetic energies of arriving particles can be greatly reduced by introducing an additional background gas to thermalize the plume, which we call th-PLD (Fig. 1). The energetic process uses parameters similar to previous studies of the homoepitaxy of $SrTiO_3$ [6]. A background gas of 2 mTorr O_2 is used to ensure proper oxidation of the growing surface. The substrate temperature is 600 °C, resulting in extended layer-by-layer growth. For the thermalized process [7], 300 mTorr of helium buffer gas is added along with the oxygen. Helium thermalizes the plume without inducing the production of nanoparticles. Time-of-flight curves obtained with a Langmuir probe for each process are shown in Figs. 1(c) and 1(d) [8,9]. For these measurements the sample was replaced by a probe than can be placed at various target-to-probe distances. At high helium background pressure the fast component shown in Fig. 1(c) is completely replaced with a much slower component, as shown in Fig. 1(d). As a result, particle kinetic energies are reduced from $\approx$100 eV/atom for e-PLD to $\approx$0.2 eV/atom for th-PLD. However, we note that the pulse intensity σ is the same for e-PLD and th-PLD within 20% across all deposition runs.

Real time x-ray scattering with a photon energy of 11.35 keV is performed during the growth to extract in-plane and out-of-plane structural information about the growing films, as shown in Figs. 1(a) and 1(b). The measurements are done at the [0 0 1/2] anti-Bragg position to maximize sensitivity to single unit cell height features. A broad component of diffuse scattering is visible corresponding to unit-cell height islands on the surface. This image corresponds to 5 ML of deposition with a dwell time of 6 s, which results in a relatively coarse array of islands. The scattering forms a nearly perfect circle with a radius of $\approx$0.2 nm^{-1}, indicating that islands are isotropically arranged on the surface with a mean spacing of $\approx$30 nm. In our experiments, we are sensitive to in-plane diffuse scattering intensity out to about 3 nm^{-1}, corresponding to length scales on the order of 2 nm. That is, we can access the whole range of length scales over which the two-dimensional islands form, from the scale of newly arrived particles in individual laser pulses through the aggregation, coarsening, and coalescence stages of monolayer growth as they occur.
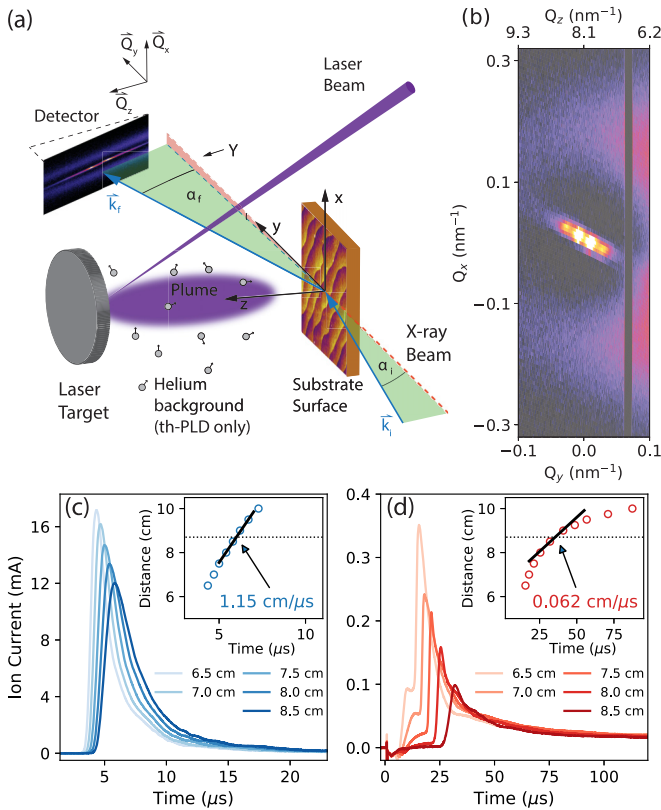
[*]rheadrick@uvm.edu

FIG. 1. (a) Schematic of the x-ray scattering experiment and th-PLD process. The th-PLD process differs from e-PLD only in that partial thermalization of the laser plume is accomplished by introducing 300 mTorr of helium into the growth chamber. (b) A portion of the scattering pattern transformed into Q coordinates. (c) Time-of-flight (TOF) spectra for positive ions in the e-PLD process at several target-to-probe distances. (d) The corresponding TOF for th-PLD. The insets in (c) and (d) show the arrival times of the leading edge of the laser plume versus distance. The slope of the curve at the target-to-sample distance of 8.7 cm gives the laser plume velocity when it reaches the sample.

Previous research on atomic-scale mechanisms has focused on the possibility that arriving particles with hyperthermal kinetic energies in the range of tens to hundreds of electron volts typical of PLD produce energetic surface smoothening effects, including energetic-particle island breakup and nonthermal transient enhanced mobility. Transient enhanced mobility is thought to involve conversion of hyperthermal kinetic energy into ballistic motion of deposited species [10–12]. The motion can be in-plane—like enhanced surface diffusion—or it can involve material transferring between layers, such as when material lands on top of a unit-cell height island and then hops over the step edge to the next lower terrace. For example, it was observed in several experimental x-ray scattering studies of SrTiO3 homoepitaxy that interlayer transport occurs on two different time scales separated by orders of magnitude [10,11].

An additional energetic mechanism was suggested by Willmott *et al.* [13] for PLD growth of La$_{1-x}$Sr$_x$MnO$_3$ on SrTiO$_3$, in which the energetic species in the laser plume breaks up islands into smaller daughter islands. Island breakup is

expected to delay the average island size from reaching the critical size at which the next layer begins to nucleate. This delay should lead to a relatively smoother growth surface. These results seem to confirm computational predictions of a breakup effect in which adatoms are "chipped" from the edges of larger islands [14]. Supporting evidence has also been found in an experimental study of platinum homoepitaxy by PLD, in which deposited particles with energies above 200 eV result in a higher island nucleation density, attributed to an increase of adatoms pushed out of the surface by the impinging energetic particles [15]. On the other hand, later studies of SrTiO$_3$ homoepitaxy utilizing x-ray scattering measurements sensitive to in-plane structure have shown that the surface in-plane length scale increases significantly during the growth [16,17]. This was interpreted as evidence that significant island breakup does not occur.

As we have mentioned above, we define the PLD regime as being the case where all the material in the laser plume is deposited before it diffuses significantly or nucleates islands, so that in the absence of fast nonthermal processes the instantaneous pulse (impulse) approximation is valid. This has important implications for the length scale of the islands, particularly during the initial stages of recovery after a deposition pulse. In continuous deposition the peak island density scales as F^χ where F is the deposition flux and χ is an exponent that depends on the size of the critical nucleus [18]. On the other hand, in PLD the nucleation density in the impulse approximation is set by the pulse intensity σ, with a length scale of $\ell \approx a/\sigma^{1/2}$, where a is the lattice constant [19]. The arrival time for the main part of the plume is $\Delta t < 10^{-4}$ s for PLD, so that ℓ depends on σ rather than on the flux during the pulse, $F_{pulse} = \sigma/\Delta t$.

Here, we present *in situ* x-ray scattering measurements of homoepitaxial growth of SrTiO$_3$, by comparing the standard energetic deposition process (e-PLD) with a nearly thermalized version of PLD (th-PLD), as described above. We report two principal results. (i) The length scale is reduced and the nucleation density is greatly increased in e-PLD relative to th-PLD. We observe, for a pulse intensity $\sigma \approx 1/20$ ML, the in-plane length scale ℓ in e-PLD can approach the limiting value deduced above, which for $a = 0.3905$ nm is ≈ 2 nm. Coarsening is also limited during e-PLD, consistent with island breakup. (ii) We find that fast interlayer transport occurs during both processes. This result is remarkable since the kinetic energy of particles in th-PLD is reduced by more than two orders of magnitude compared to e-PLD, yet the amount of fast interlayer transport is estimated to be the same in both processes. Moreover, by result (i) th-PLD also produces larger island sizes, which implies that deposited particles have to migrate significantly longer distances to reach the nearest step edge.

Surface x-ray scattering can be divided into two contributions: (i) the specular reflection, which is only sensitive to the layer coverages, and (ii) the diffuse intensity, which is additionally sensitive to in-plane structure. Figure 2(a) shows both specular and diffuse data during e-PLD growth up to a thickness of 9 unit cells. The top panel is the specular intensity, which oscillates with each layer, indicating layer-by-layer growth. A defining characteristic of PLD is that the jumps in the specular intensity coincide with the arrival of
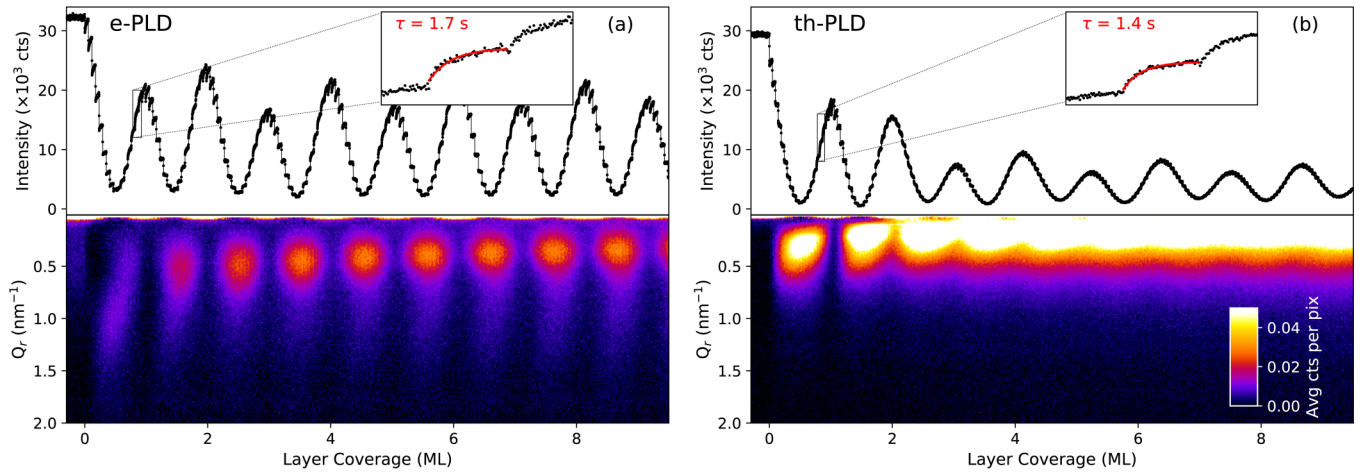
FIG. 2. Total specular and diffuse scattering comparison between the energetic process (a) and the thermalized process (b) for a 6 s dwell time. The top panels in (a) and (b) show the evolution of the total specular intensity and the bottom panels show the corresponding diffuse scattering as a function of Q_r. The insets in (a) and (b) show the thermal recovery of the specular intensity for a single pulse near 0.8 ML coverage. Note that the time axis has been converted to layer coverage for convenience, although coverage increases in discrete steps at each laser pulse.

the plume due to a sudden change in the layer coverages. After each pulse, there is a slow evolution of the intensity as monomers descend and attach to step edges from above. Comparable results for th-PLD are shown in Fig. 2(b). The specular intensity is similar aside from a slightly reduced intensity at the peaks of the oscillations. The lower panels in Figs. 2(a) and 2(b) show diffuse scattering profiles versus deposited thickness. They reveal an interesting difference that e-PLD exhibits a broad distribution centered at ≈ 1 nm^{-1} that recurs during each deposited layer without coarsening, which is absent from the th-PLD profiles. This peak position corresponds to a length scale of ≈ 5 nm. As we discuss below, the length scale of this profile can be as small as 2.5 nm for shorter dwell times. The multimonolayer regime is more complex since preexisting islands play a role. A diffuse peak appears at 0.5 nm^{-1} in e-PLD during the growth of the second ML, and gradually coarsens during subsequent growth. A similar peak occurs in th-PLD, but it appears earlier, and it is shifted to lower Q_r throughout the growth.

In order to gain further insight into this difference and its origin, Figs. 3(a) and 3(b) show diffuse scattering profiles for various dwell times at the same coverage of $\theta = 0.4$ ML. For these plots, we performed a circular average of the diffuse intensity at each Q_r, where $Q_r = \sqrt{Q_x^2 + Q_y^2}$. Background corresponding to scattering from the substrate before the deposition was also subtracted, as described in the Supplemental Material [9]. There is a clear difference in the diffuse scattering profiles, both as a function of the dwell time and also between e-PLD and th-PLD. In Fig. 3(c), we plot the length scale ℓ derived from the peak position of the diffuse scattering, $Q_{r,max}$. Comparison of the curves for energetic and thermalized deposition reveals the remarkable result that the thermal coarsening effect is inhibited in e-PLD, which implies that the nucleation density is greatly increased by energetic effects. For example, comparing the curves for 6 s dwell time in Fig. 3(c), we see that the length scale for e-PLD is about a factor of three smaller than for th-PLD over the entire range of coverages. For shorter dwell times,

where surface diffusion and relaxation are less dominant, we observe that the length scales become progressively smaller, even approaching the diffusionless limit of $\ell \approx 2$ nm that we deduced from the pulse intensity.

Based on the discussion above, the first main conclusion of this study is that the reduced in-plane length scales and coarsening rates for e-PLD are consistent with the island breakup mechanism [13,14]. This process significantly counteracts the effects of thermal surface diffusion, aggregation, and ripening, leading to an island density that can be an order of magnitude higher for e-PLD compared to th-PLD for long dwell times. However, a net coarsening still occurs for e-PLD, albeit at a slower rate, as shown in Fig. 3(c), and it continues during the first few monolayers of growth, as observed in Fig. 2(a).

The specular intensity can be expressed as a simple function of the layer coverages. Assuming layer coverages $\theta_n(t)$ for layers $n = 1$–N,

$$I(t) \propto |F(Q)|^2 \left| \frac{1}{1 - e^{iQa}} + \sum_{n=1}^{N} \theta_n(t) e^{-iQna} \right|^2, \qquad (1)$$

where $F(Q)$ is the scattering amplitude of a single unit-cell high layer and Q is the magnitude of the scattering vector, which is oriented along the surface normal for the specular reflection.

Equation (1) can be used to formulate several simple growth models for the intensity at the anti-Bragg position. In one model called the impulse approximation, it is assumed that monomers arrive at random positions on the surface during the pulse and then remain in the same layer. This model predicts a drop in specular intensity I following each laser pulse given by $\Delta I/I = -4\sigma(1 - \sigma)$ [10]. The opposite limiting case is for perfect layer-by-layer (LBL) growth, which is described by $\Delta I/I = -4\sigma[(1 - \sigma) - 2\theta]/(1 - 2\theta)^2$. Note that the impulse model predicts that the intensity jump is always negative, so that in the absence of any relaxation the intensity should continuously decrease. This is clearly inconsistent with experimental observations of an oscillating
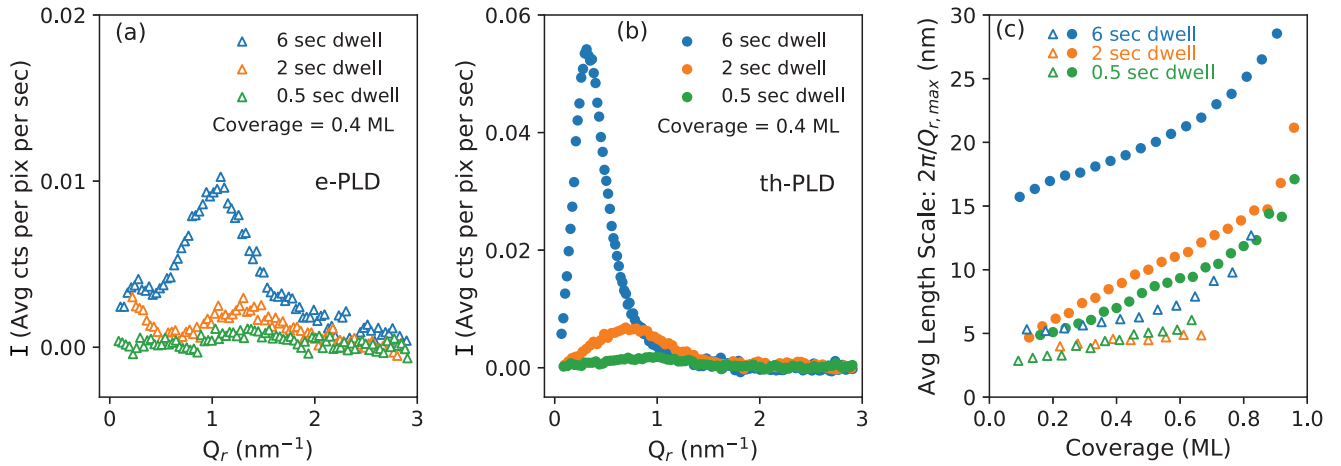
FIG. 3. Diffuse scattering profiles averaged over a single pulse at 0.4 ML coverage during the first monolayer of growth for (a) the energetic process and (b) the thermalized process. (c) Average length scale during the first monolayer of deposition. The triangles are for e-PLD and the circles are for th-PLD.

intensity during growth. Therefore, interlayer transport must occur following each laser pulse, and so the interesting question becomes on what time scale does it occur? In order to address this question, Fig. 4 shows plots of the experimental fast intensity jump along with the total change in the intensity after the dwell time (labeled "Jump + recovery") for each pulse during the first monolayer of deposition. The results show that the fast jump amplitude significantly deviates from the impulse model. This is evidence that there must be a fast relaxation component, a result that was previously deduced for e-PLD [10]. Interestingly, the fast jump amplitudes (blue symbols in Fig. 4) are almost the same for th-PLD and e-PLD, which is remarkable since previous work emphasized the possible role of high kinetic energies ($E_k \gtrsim 10$ eV) in promoting interlayer transport [10,11]. In contrast, our results show that the high kinetic energy of the incident particles in e-PLD does not enhance interlayer transport relative to the more modest energies present in th-PLD. The data for

the intensity change after the dwell time is observed to be closer to the LBL model. Thus thermal relaxation also plays a significant role although it occurs on a much slower time scale.

The second main conclusion of this study is that fast interlayer transport occurs for th-PLD as well as e-PLD. We note that based on our Langmuir probe time-of-flight studies the temperature of incident particles in th-PLD may be as high as 1500 K. In this range, "hot" particles incident in normal incidence can scatter nearly elastically from surface atoms, leading to a significant velocity in the plane of the surface. For example, computational results by Gao *et al.* for Pd deposition on MgO showed that Pd arriving near Mg surface atoms can recoil with a significant lateral velocity without desorbing [20]. Particles incident with 0.4 eV kinetic energy were found to travel up to 2 nm from their impact site. Our results indicate that partially thermalized particles in $SrTiO_3$ th-PLD travel up to ≈ 5 nm during growth.

In conclusion, our results suggest that incident particles with kinetic energies $0.1 < E_k < 10$ eV can migrate via transient-enhanced surface diffusion. Higher kinetic energies can break chemical bonds, leading to phenomena such as island breakup. These mechanisms should be included in models of epitaxial growth by hyperthermal and energetic deposition methods and they can be exploited to engineer thin films and multilayers with improved properties.
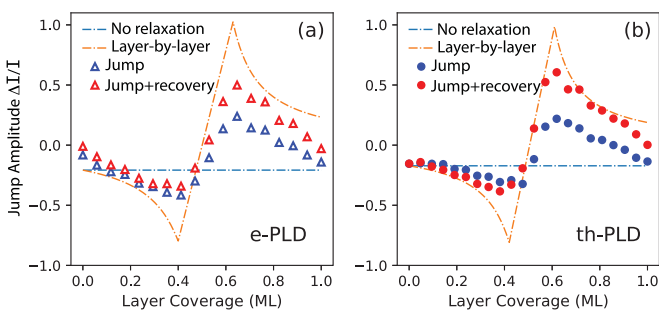
FIG. 4. Analysis of the transient jump in the specular intensity following each laser pulse for (a) e-PLD and (b) th-PLD. Blue symbols labeled "Jump" represent the immediate normalized intensity change, while the symbols labeled "Jump + recovery" represent the total normalized intensity change at the end of the 6 s dwell time. The lines are the two limiting cases of random deposition with no interlayer relaxation (blue) and perfect layer-by-layer relaxation (orange).

[1] E. Vasco, C. Polop, and J. L. Sacedón, Phys. Rev. Lett. **100**, 016102 (2008).

[2] A. Ohtomo and H. Hwang, Nature (London) **427**, 423 (2004).

[3] N. Reyren, S. Thiel, A. Caviglia, L. F. Kourkoutis, G. Hammerl, C. Richter, C. Schneider, T. Kopp, A.-S. Rüetschi, D. Jaccard *et al.*, Science **317**, 1196 (2007).

[4] A. Caviglia, S. Gariglio, N. Reyren, D. Jaccard, T. Schneider, M. Gabay, S. Thiel, G. Hammerl, J. Mannhart, and J.-M. Triscone, Nature (London) **456**, 624 (2008).

[5] H. N. Lee, H. M. Christen, M. F. Chisholm, C. M. Rouleau, and D. H. Lowndes, Nature (London) **433**, 395 (2005).

[6] G. Eres, J. Z. Tischler, C. M. Rouleau, P. Zschack, H. M. Christen, and B. C. Larson, Phys. Rev. B **84**, 195467 (2011).

[7] B. Shin and M. J. Aziz, Phys. Rev. B **76**, 085431 (2007).

[8] B. Doggett and J. G. Lunney, J. Appl. Phys. **105**, 033306 (2009).

[9] See Supplemental Material at http://link.aps.org/supplemental/10.1103/PhysRevB.101.241406 for details of the Langmuir probe method and the x-ray diffuse scattering background subtraction.

[10] A. Fleet, D. Dale, Y. Suzuki, and J. D. Brock, Phys. Rev. Lett. **94**, 036102 (2005).

[11] J. Z. Tischler, G. Eres, B. C. Larson, C. M. Rouleau, P. Zschack, and D. H. Lowndes, Phys. Rev. Lett. **96**, 226104 (2006).

[12] E. Vasco and J. L. Sacedón, Phys. Rev. Lett. **98**, 036104 (2007).

[13] P. R. Willmott, R. Herger, C. M. Schlepütz, D. Martoccia, and B. D. Patterson, Phys. Rev. Lett. **96**, 176102 (2006).

[14] J. M. Pomeroy, J. Jacobsen, C. C. Hill, B. H. Cooper, and J. P. Sethna, Phys. Rev. B **66**, 235412 (2002).

[15] M. Schmid, C. Lenauer, A. Buchsbaum, F. Wimmer, G. Rauchbauer, P. Scheiber, G. Betz, and P. Varga, Phys. Rev. Lett. **103**, 076101 (2009).

[16] G. Eres, J. Z. Tischler, C. M. Rouleau, H. N. Lee, H. M. Christen, P. Zschack, and B. C. Larson, Phys. Rev. Lett. **117**, 206102 (2016).

[17] J. D. Ferguson, G. Arikan, D. S. Dale, A. R. Woll, and J. D. Brock, Phys. Rev. Lett. **103**, 256103 (2009).

[18] J. A. Venables, G. D. T. Spiller, and M. Hanbucken, Rep. Prog. Phys. **47**, 399 (1984).

[19] B. Hinnemann, H. Hinrichsen, and D. E. Wolf, Phys. Rev. Lett. **87**, 135701 (2001).

[20] D. Z. Gao, M. B. Watkins, and A. L. Shluger, J. Phys. Chem. C **116**, 14471 (2012).